


Quantitative assessment and optimization of bi-functional membrane for remediation of Cr(VI) from wastewater

Zeenat Arif ^{a,*} and Naresh Kumar Sethy^b

^a Chemical Engineering Department, Harcourt Butler Technical University, Nawabganj, Kanpur, UP, India

^b Department of Chemical Engineering and Technology, Indian Institute of Technology (BHU) Varanasi, Varanasi, UP, India

*Corresponding author. E-mail: zeenata.rs.che15@itbhu.ac.in

 ZA, 0000-0002-4748-0254

ABSTRACT

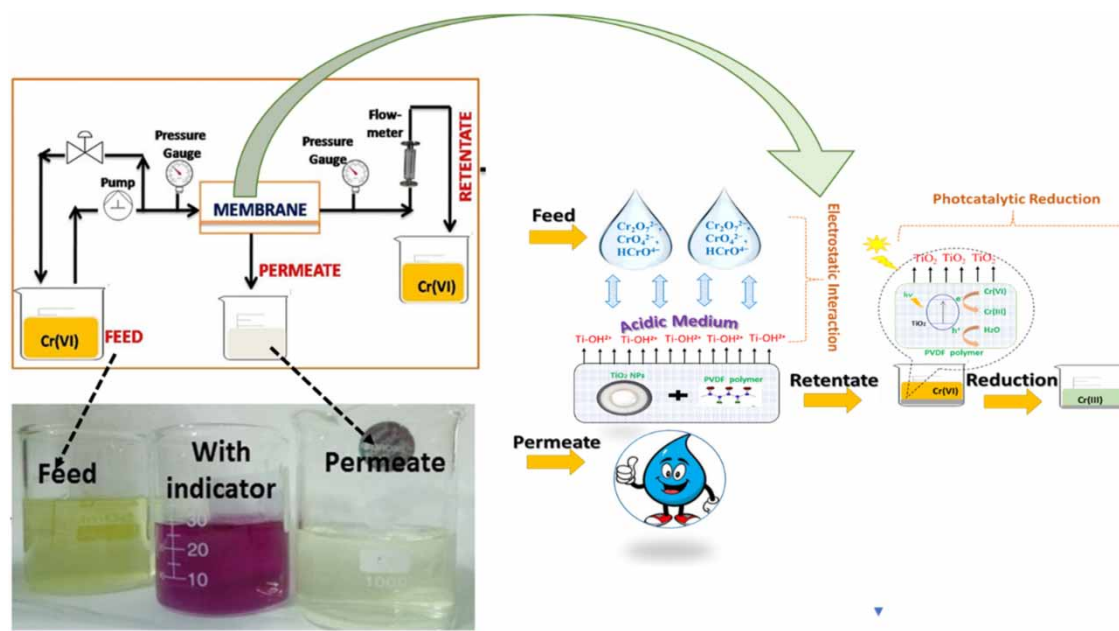
This paper explores the innovative approach of using a green route synthesized cost-effective bi-functional to eliminate toxic hexavalent chromium commonly found in tannery wastewater by using an integrated application of membrane and photocatalyst. Contaminated wastewater is firstly passed through bi-functional ultrafiltration membranes to retain hexavalent chromium and further reducing the toxicity of rejected water having high concentrations of Cr(VI) by photocatalytic reduction into Cr(III) in the presence of sunlight using the same membrane as photocatalyst film. Conditions governing the separation process such as solution pH, nanoparticle loading in polymer matrix, and concentration of Cr(VI) have been optimized to maximize the % rejection and photocatalytic reduction to Cr(III). The purpose of this work was to optimize the process condition through the use of the response surface method (RSM) that governs the process. RSM analysis concludes that excellent rejection of 91.58% and reduction of 87.02% is possible at the predicted pH (5.55), particle loading (2.14%) and Cr(VI) concentration (25 mg/L).

Key words: concentration, hexavalent chromium, membrane, photocatalyst, reduction, rejection

HIGHLIGHTS

- Synergistic approach for Cr(VI) removal by membrane followed by photocatalytic degradation.
- Response surface methodology was employed to optimize the parameter governing operation of a bi-functional membrane.
- Rejection >90% was achieved using as bi-functional membrane under optimum conditions.
- Reduction >85% when used as photocatalysis film.
- BET Brunauer–Emmett–Teller results confirm membrane recyclability as it retains its properties after application.

GRAPHICAL ABSTRACT



INTRODUCTION

A highly toxic heavy metal i.e. chromium, exists as trivalent chromium Cr(III) and hexavalent chromium Cr(VI). The Cr(VI) is environmentally more hazardous compared to Cr(III) and is harmful not only for human life but also flora and fauna (Jyothi *et al.* 2017). It holds a position in the top 20 contaminants list of hazardous substances. The major sources for the discharge of Cr(VI) into water bodies are tanning industries, metal finishing, electroplating, etc. (Zhang *et al.* 2020). Considering its harmful impact on the environment the country governments and regulatory organizations are applying strict regulation on industries to limit the discharge of Cr(VI)-bearing wastewater. The different organizations had defined the limit of chromium concentration in water for e.g. the United States Environmental Protection Agency (USEPA) has set the maximum contamination level (MCL) of 100 µg/L in drinking water, conversely the maximum concentration of 50 µg/L was recommended by the World Health Organization (WHO) (Arif *et al.* 2020a). So it has become the first priority to reduce and control the toxicity level of Cr(VI) to a permissible value before discharge into water bodies. Various existing conventional technologies like adsorption, ion exchange, and electrochemical reduction used for the elimination of Cr(VI) have several drawbacks like ineffective removal of metal at low concentrations, increased volume of sludge generation and difficulty in their disposal (secondary pollutant generation), high chemical consumption, relatively high operational cost, non-destructive processes, and incompatibility for large-scale application are their major limitations (Burakov *et al.* 2018; Crini & Lichtfouse 2019).

In comparison, different emergent technologies for e.g. ion-exchange, electro-dialysis, reverse osmosis, and nanofiltration photocatalysis are known for their excellent removal capacity and low volume of sludge production, but these techniques are either expensive, complex (Arif *et al.* 2020b) and have a poor recover ability when using direct photo-catalysts that limits its successful application and adds additional cost to the system (Jyothi *et al.* 2017). In contrast, developed photocatalytic membrane technology that incorporates the synergistic properties of both organic and inorganic materials does not need any consumption of hazardous chemicals and removes contaminants (toxic metals) from wastewater using membranes without generating any harmful product, because it is further used as a photocatalyst film for retreating the retentate (feed wastage) using the same membrane material. The developed photocatalytic membrane involves immobilization of catalytic materials on a polymer matrix. The combination of organic and inorganic materials will not only enhance the material reusability but also eliminate the generation of a secondary pollutant.

Among the various membrane separation processes, ultrafiltration (UF) is used widely because of its low energy requirement when compared with nano-filtration (NF) and reverse osmosis (RO). The membranes composed of polymer matrix

like polyvinyl alcohol are relatively inexpensive but suffer from poor stability, so polyvinylidene fluoride (PVDF) is the widely used polymer material for UF applications because of its outstanding resistivity to harsh chemicals (Arif *et al.* 2019a), but being hydrophobic in nature adversely affects the membrane performance. Different techniques had been adopted to circumvent this problem like graft polymerization, chemical grafting, physical blending etc., but poor bonding between the host matrix and filler reduces the life span of the synthesized composite material (Arif *et al.* 2019b). For many years, immobilization of nanoparticles (NPs) (photo-catalysts) into polymer matrix has gained interest because this not only enhances the separation properties but also improves the self-cleaning properties of the membrane. Among different nanoparticles, nano-sized titanium dioxide (TiO₂) is preferred more as an inorganic filler, because of its superhydrophilicity and high catalytic activity (Ramasundaram *et al.* 2016; Sharma *et al.* 2017).

In view of this, an attempt has been made to conduct an experiment to treat chromium-bearing wastewater using synthesized PVDF/TiO₂ ultrafiltration photocatalytic membranes with different loadings of green synthesized TiO₂. NPs embedded in PVDF polymer were prepared to be used as a photocatalytic membrane to eliminate toxic Cr(VI) from wastewater and reduce it to Cr(III). This integrated approach minimizes the generation of waste in the form of membrane retentate and thus reduces the human capital without compromising its efficiency. There is insufficient published information in the open literature on the use and performance of bi-functional photo-catalyst membranes for the rejection and reduction of Cr(VI) species at different operating conditions. Using the first-time extract of *Cajanus cajan* to obtain titanium dioxide as a filler in a polymer matrix to enhance the efficiency of membranes and reduce the toxic hexavalent chromium to non-toxic trivalent chromium is the novelty of this paper. The presence of functional groups like terpenoids, aliphatic and aromatic amines in *Cajanus cajan* helps in stabilization and avoids the agglomeration of NPs. At the same time, a mathematical tool, the response surface methodology (RSM), has been used for the first time to optimize the operating parameters governing the operation of a bi-functional membrane. This methodology reduces the number of experiments and optimizes the parameters to achieve our goal i.e. maximum rejection and reduction using the same material.

MATERIALS AND METHODS

Materials

Potassium dichromate and diphenylcarbazide were purchased from Merck (Bombay), double-distilled (DD) water prepared in the laboratory was used in all experiments.

Membrane synthesis

The composite membranes of PVDF/TiO₂ were synthesized by a phase-inversion method. Homogeneous polymeric solution was prepared using pre-dried PVDF pellets (90 °C for 24 h) and organic solvent *N*-methyl-2-pyrrolidone (NMP) at a ratio of 1:5 (wt/volume) in a magnetic stirrer at 70 °C. Simultaneously, suspensions of synthesized TiO₂ in different weight proportions were prepared in NMP solvent (4 ml) by sonication each for 1 h and thereafter was mixed with prepared PVDF solution thoroughly with continuous stirring for 8 h at 70 °C. The resulting solution was then cast on a glass film applicator with a clearance of 200 μm and exposed to an ambient environment for very short duration of 30 min to achieve partial evaporation of the solvent and immediately then placed in a water bath maintained at temperature (27 ± 1 °C) for 24 h to allow precipitation. Finally, developed membranes were peeled off, washed and remain immersed in water for further study.

Membrane performance

The simple hydrolysis mechanism was the reason behind the formation of nanoparticles using *Cajanus cajan* extract and the concept of phase inversion led to the formation of the membrane. The detailed synthesis procedure for TiO₂ nanoparticles (NPs) and PVDF/TiO₂ composite membrane is reported in the authors' published literature (Arif *et al.* 2020a). To understand the effect of NP loading on the performance of the photocatalytic ultrafiltration membrane, the amount of particles with respect to the polymer was varied and is marked as M1 (0 wt%), M2 (1 wt%), M3 (2 wt%), M4 (3 wt%).

Rejection of Cr(VI)

The separation experiments were performed using the membrane setup as shown in Figure 1. The synthesized membranes were uniformly cut providing a filtration area (A) of 12.56 m² and were mounted on the membrane holder made up of stainless steel and sealed with an O-ring to avoid leakage. Initially membranes (M1 (0 wt%), M2 (1 wt%), M3 (2 wt%), M4 (3 wt%)) were compacted at 0.5 bar for 1 h to achieve a stable flux at the ambient temperature. The membrane set up was also provided

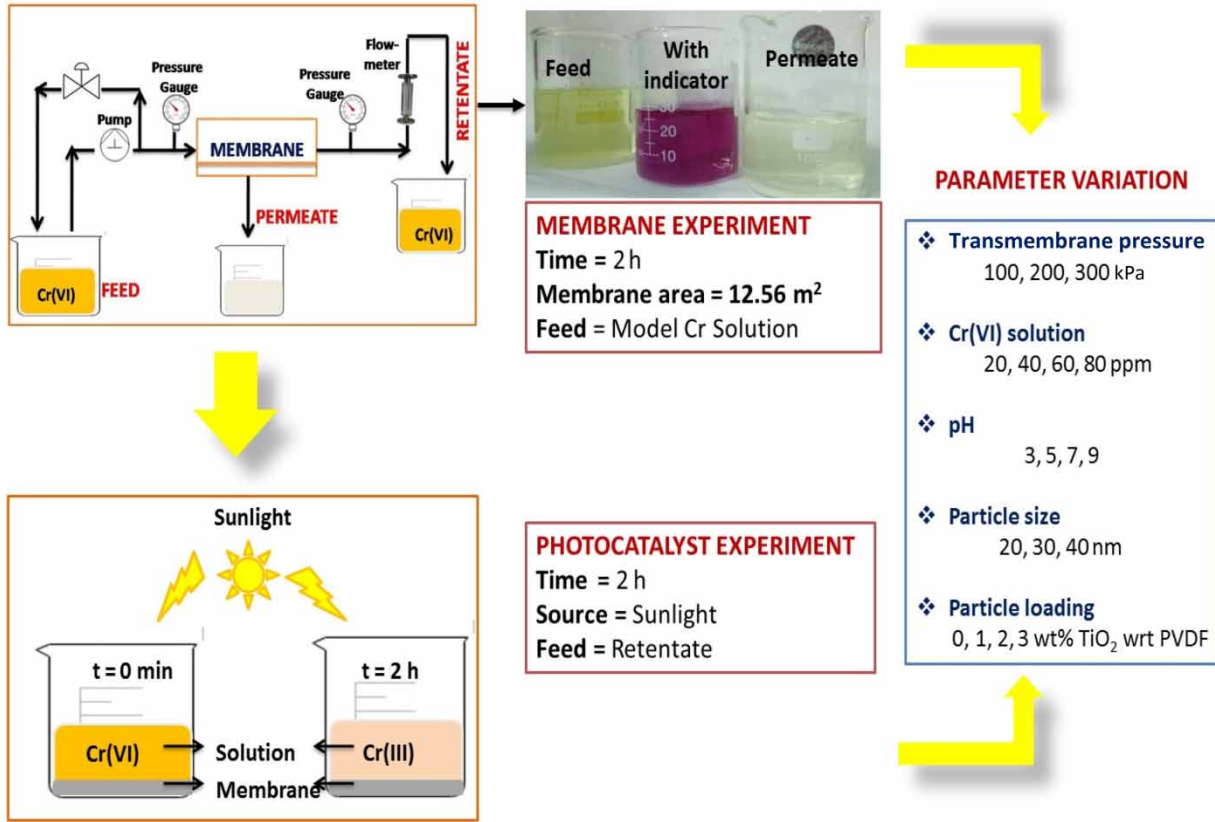


Figure 1 | Schematic representation of setup for rejection of Cr(VI) using a membrane and the reduction of Cr(VI) using a photo-catalyst.

with a feed glass vessel with a magnetic stirrer for holding dichromate solution (chromium solution made from potassium dichromate (20, 40, 60, 80 ppm, 500 ml) at different pH (3, 5, 7, 9), and transmembrane pressure (100, 200, 300 kPa). The flux Q_w (L/m^2h) was calculated by measuring the filtrate for 2 h and using Equation (1):

$$Q_w = V_p / (A \times t) \tag{1}$$

where V_p is the mass of permeate (L), and t is the permeation time (h).

% Rejection was calculated using Equation (2):

$$\% \text{ Rejection} = (1 - C_p / C_f) \times 100 \tag{2}$$

where C_f and C_p are the chromium concentrations in the feed and permeate, respectively.

The concentration of chromium was evaluated using method described in *Lace et al. (2019)*.

Photocatalytic reduction of Cr(VI)

After 2 h, retentate bearing the concentrated chromium was collected in a 500 ml beaker with a used PVDF/TiO₂ composite membrane piece at the bottom and was subjected to photocatalytic reduction under sunlight. Here, 10 ml aliquots were collected at regular intervals and analyzed for Cr(VI). Reduction experiments were also conducted for all samples of retentate obtained under different operating conditions (pH, Cr(VI) concentration, pressure, particle loading and size). The % reduction was evaluated using Equation (3):

$$\% \text{ Reduction} = (1 - C_{rp} / C_{rf}) \times 100 \tag{3}$$

where C_{rf} and C_{rp} are the chromium concentrations at $t = 0$ min and $t = t$ min, respectively.

Membrane porosity and pore radius

The membrane porosity (ε) was evaluated using a gravimetric method. Dried membrane strips of definite dimension (1 cm \times 1 cm) were weighed initially (W_d) and then immersed in water for 1 h. After a 1 h interval, strips were taken off, blotted with paper, and weighed again (W_w). The porosity value was calculated using the simple equation mentioned below:

$$\varepsilon = \frac{W_w - W_d}{a \times l \times \rho_w} \quad (4)$$

where a is membrane area (m^2), membrane thickness is designated as l and ρ_w represents water density.

Pore size (r) of the membrane was calculated using Equation (5):

$$r_m = \sqrt{\frac{(2.9 - 1.7\varepsilon) \times 8\mu_w \times l \times Q}{\varepsilon \times a \times \Delta P}} \quad (5)$$

where μ_w is water viscosity (8.90×10^{-4} Pa.s)

Analysis of Cr(VI) concentration

The Cr(VI) concentration was measured using the 1,5 diphenylcarbazide method using a PC-based double beam spectrophotometer (SYSTRONICS, PC Based Double Beam Spectrometer 2202, India). An aliquot (5 ml) containing Cr(VI) solution was diluted to 95 ml using deionized water. Next, 0.25 g of 1,5-diphenyl carbazide in 50 ml methanol was prepared, from which 500 μ L was added to 5 ml of prepared Cr solution and pH was maintained at 2 ± 0.5 using H_2SO_4 solution (Lace *et al.* 2019). After 5 min, the absorbance of the purple color solution was measured by an ultraviolet (UV) light spectrophotometer at 560 nm. Initially a calibration curve was prepared using standard dichromate solutions and then the unknown solution concentration was evaluated using the standard plot.

Response surface methodology and optimization analysis

Experimental design

The RSM is a widely used optimization and analysis tool to reduce the number of experiments as well as incorporating all the interacting parameters that were earlier missing in conventional techniques (Arif *et al.* 2020a). Central composite design (CCD), standard RSM design was selected to study the influence of pH, chromium concentration, and particle loading (independent variables) on the chromium rejection and reduction from aqueous solution (dependent variables). The ranges of the above parameter were varied as: pH 5–8, Cr(VI) concentration 20, 40, 60, and 80 mg/L and particle loading (0 wt%, 1 wt%, 2 wt% and 3 wt%). These three prime process variables were examined rigorously and were optimized using the RSM Design Expert version 8.0 software since they severely affect the dependent variables. The optimized values of process variables were evaluated at the maximum value of rejection and reduction as this will be considered as the main goal. The design includes 20 experimental trials and six centre points, as shown in Table 1, in order to maintain the accuracy. Equation (4) will determine the experiment number (N):

$$N = 2^n + 2n + n_c \quad (6)$$

where n and n_c signify the number of independent variables and the number of replicates (centre point), respectively, thus the value of N obtained using software is 20.

A second-order polynomial equation was applied which includes both the quadratic and interaction terms obtained from the CCD model to optimize the independent variables for the % rejection and % reduction (responses) obtained from experiments. The mathematical expression for the second-order equation can be written as shown in Equation (5):

$$r_y = \beta_0 + \sum_{i=1}^m \beta_i x_i + \sum_{i=1}^m \beta_{ii} x_i^2 + \sum_{i < j}^m \beta_{ij} x_i x_j \quad (7)$$

where response is represented by r_y , coded values are x_i and x_j , coefficients β_0 , β_i , β_{ii} , and β_{ij} signify regression, linear, quadratic, and interaction terms, limit 'm' represents number of the design variables. To check the reliability of the equation,

Table 1 | CCD experimental matrix design for Cr(VI) removal using composite membrane

Runs	pH	Particle loading	Concentration (mg/L)	Rejection (%)	Reduction (%)
1	3	0	20	6.01	12.5
2	3	3	20	88.03	80.25
3	3	0	80	4.98	11.37
4	3	3	80	85.4	76.98
5	8	0	20	5.9	11.31
6	8	3	20	81.02	72.1
7	8	0	80	5.4	11.24
8	8	3	80	79.1	70.25
9	5.5	0	50	5.54	11.5
10	5.5	3	50	86.54	76.98
11	5.5	1.5	20	90.14	85.25
12	5.5	1.5	80	87.03	70.2
13	3	1.5	50	89.99	75.5
14	8	1.5	50	87.48	71.99
15	5.5	1.5	50	88.32	74.98
16	5.5	1.5	50	88.32	74.98
17	5.5	1.5	50	88.32	74.98
18	5.5	1.5	50	88.32	74.98
19	5.5	1.5	50	88.32	74.98
20	5.5	1.5	50	88.32	74.98

Analysis of Variance (ANOVA) was employed. We also determined the other statistical fitness of the model such as determination coefficient (R^2), adjusted determination of coefficient (R_{adj}^2), degree of freedom, F and p -value.

Validation

An experiment was conducted for the condition of optimum values suggested by RSM using an ultra-filtration setup. Details of the filtration setup are already mentioned above. After achieving stable flux when the membrane was pre-pressurized for 30 min, 500 ml of Cr(VI) solution at the suggested optimum condition was passed through the membrane. Chromium concentrations on both side of the membrane were evaluated and the obtained concentrated chromium (VI) on the retentate side underwent photocatalytic reduction in the presence of sunlight.

Regeneration of nanocomposite membranes

Material stability and reusability are important factors for its commercialization at large scale. Running the experiments five times at the optimized conditions with same membrane material is one of the simplest methods to estimate its reusability capacity. After each run, the used membrane piece was simply washed with Millipore water to remove any residual substance from it and was reused. To analyse any morphological changes in the membrane, the membrane was characterized using Fourier transform infrared (FTIR) spectroscopy and a Brunauer–Emmett–Teller (BET) surface area analyzer before and after the completion of the experiment.

RESULTS AND DISCUSSION

Cr(VI) removal using bi-functional membrane from wastewater: mechanism

TiO₂ particles and Cr exist in acidic and alkaline media. Different forms of Cr are Cr₂O₇²⁻, CrO₄²⁻, HCrO₄⁻ in acidic and H₂CrO₄ in basic aqueous solution, whereas the protonation and deprotonation of hydroxyl groups generates Ti-OH₂⁺ in acidic conditions and Ti-OH⁻ in the basic environment on the surface of particles due to the amphoteric nature of the TiO₂ particles. Hence it implies that particles in the acidic medium adsorb anions of Cr due to the electrostatic interaction

between Cr and TiO₂ NPs, which is the main reason for the Cr(VI) rejection from wastewater while using TiO₂/PVDF as a membrane material. The same membrane material when applied as photo-catalyst film reduces concentrated Cr(VI) present in the retentate to Cr(III) through a photocatalytic process because the photons emitted upon irradiation with sunlight are absorbed by NPs and generate electron hole pairs as e^{-CB} and h^{+VB} which further reduces Cr(VI) to Cr(III), as shown Figure 2(a).

Membrane characteristics

Figure 2(b) shows the increase in porosity with increase in particles loading because of the presence of hydrophilic particles TiO₂ with high surface area. Thermodynamic and kinematic studies of composite membrane explain that with increase in

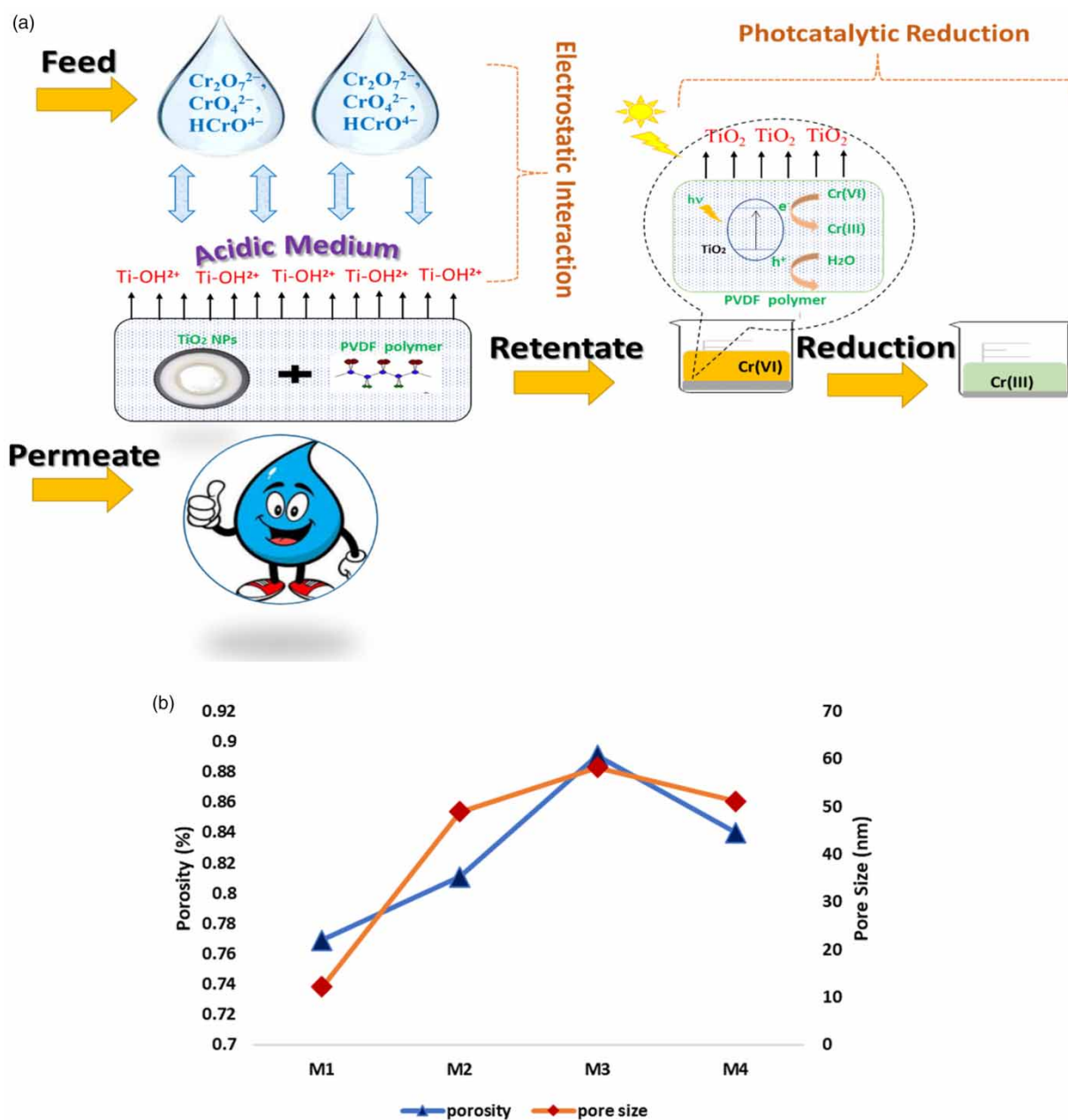


Figure 2 | (a) Mechanism for Cr(VI) removal using bi-functional membrane. (b) Porosity and pore size of the composite membrane.

particle loading, the thermodynamic factor increases, which enhances the formation of the porous structure (Arif *et al.* 2020b). Membranes with highest particle loading (M4) porosity and pore size decrease, attributed to the reduction in mass transfer rate between solvent (NMP) and non-solvent (water) during the phase-inversion process of the composite membrane because of increased casting solution viscosity with the addition of TiO₂ NPs.

UV spectra of Cr(VI) at feed, permeate, retentate and reduction side

The UV spectra of the model Cr solution are shown in Figure 3(a)–3(d) and depict that the absorbance value of Cr(VI) in the permeate is very small compared to the absorbance of Cr(VI) in the feed, as expected, since the membrane does not allow the Cr(VI) ions to pass through it due to the ionic interaction between membrane and Cr ion at acidic pH, as a result the absorbance value in the permeate is small. Also, the absorbance value of the retentate (Figure 3(c)) is higher than in the feed (Figure 3(a)) which implies that Cr(VI) is concentrated at the retentate side with time, so its absorbance value is higher at the feed side. Similarly, it is seen from Figure 3(d) that after the reduction process the absorbance value decreases with time in the presence of the nanocomposite membrane on exposure to light due to the photocatalytic reduction of Cr(VI).

Membrane adsorption capacity

Membrane pore radius directly influences adsorption mechanism, and allows only those molecules to diffuse into membrane interstitial sites which have a molecular weight less than the molecular cut-off and this phenomenon determines the available adsorption sites at membrane surface. As concluded, a membrane with 2.0 wt% dosage shows excellent result, therefore the adsorption capacity of this membrane was studied. It was observed that in first 15 min maximum adsorption was recorded

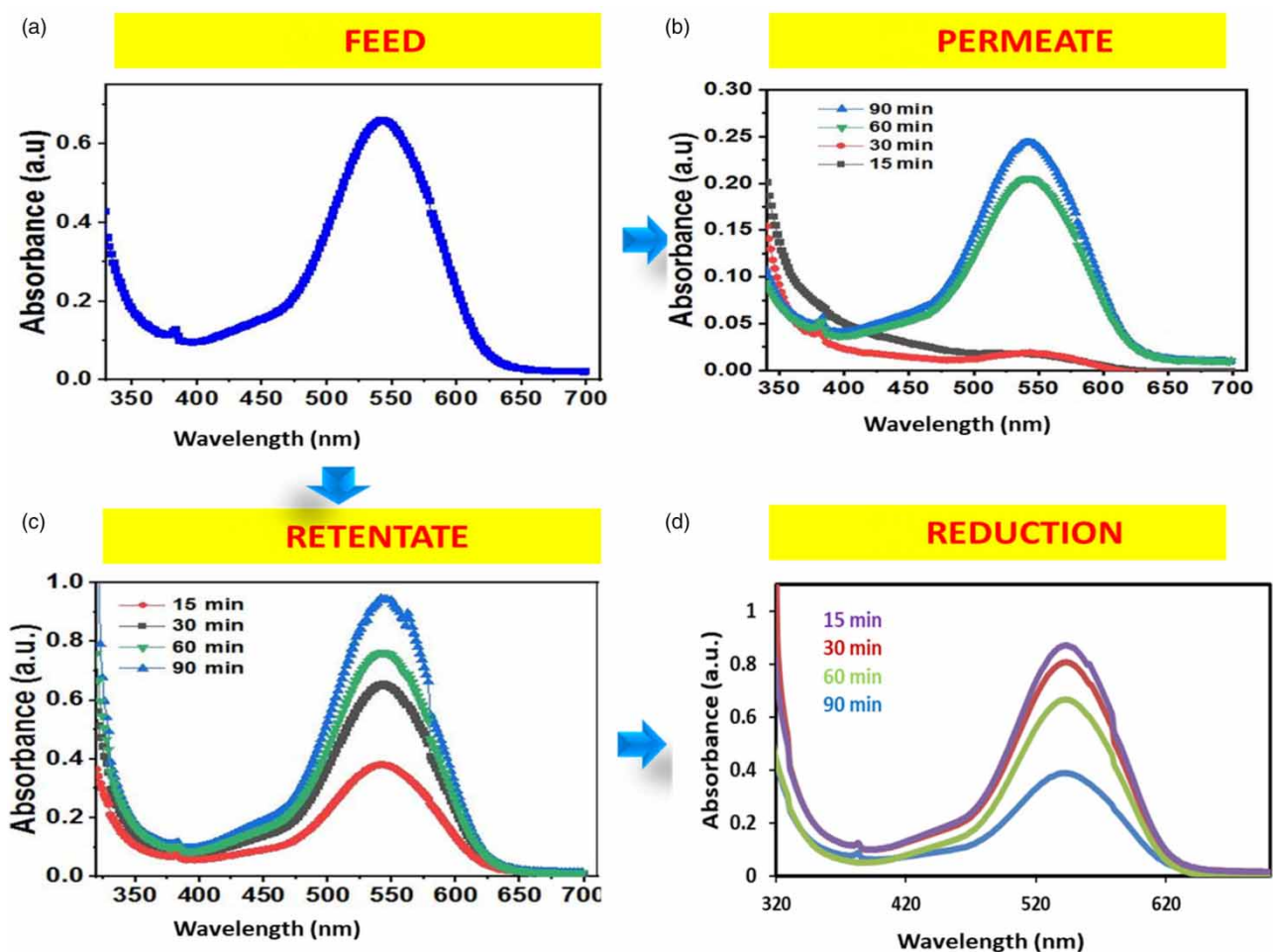


Figure 3 | UV spectra of the Cr(VI) solution. (a) Feed. (b) Permeate. (c) Retentate. (d) Reduction.

with the capacity of 2.1 g/m^2 attributed to the large number of available active sites, a similar trend was also reported by [Abba et al. 2021](#). Thereafter a decline in the adsorption capacity was observed due to membrane fouling. The adsorption capacity was evaluated using the equation as $\text{adsorption capacity} = [(C_i - C)/A] \times v$ ([Arif et al. 2019b](#)), where C_i and C represent the initial and final concentrations of chromium by placing the membrane in a beaker with the chromium solution for 12 h and A and v are membrane area and sample volume taken.

Effect of various parameters

Effect of TiO_2 particle loading on PVDF membrane

[Figure 4](#) depicts the effect of TiO_2 particle loading (wt%-0%, 1%, 2%, 3%) with respect to the PVDF polymer on the performance of the nanocomposite membrane at pH 5, transmembrane pressure (ΔP) 300 kPa, $[\text{Cr(VI)}]$ 20 ppm and particle size 20 nm. [Figure 4\(a\)](#) depicts that the flux increases from 50 to 280 $\text{L/m}^2\text{h}$ as the particle loading was increased from 0 (M1) to 2 wt% (M3). This result was expected because of the presence of hydrophilic TiO_2 NPs, these will attract more molecules of water to pass through it, also particle incorporation increases the porosity, which will ultimately result in an increase in the water flux ([Arif et al. 2020a](#)). However, particle aggregation at an excess loading of 3 wt% (M4) led to a reduction in the porosity and thus a flux value decline. A similar trend was also observed for the % rejection as shown in [Figure 4\(b\)](#) where the lowest % rejection (<10%) was obtained for the M1 membrane with no particle loading and the highest value (>90%) was obtained for the M3 membrane. The increased concentration of particles increased the number of active sites on the membrane, thereby inducing an increased electrostatic interaction between the membrane surface and Cr(VI) ions. This increased interaction will not allow the Cr ions to pass through the membrane, rather they will be rejected on the retentate side and therefore the value of rejection will increase with increase in the particle loading. For the M4 membranes, the particle aggregation reduces the number of active sites, therefore the electrostatic interaction between membrane and Cr(VI) ions will be less compared with the M3 membrane and the rejection will decrease, however, it is still higher.

The increase in concentration of NPs from 0 to 2 wt% increased the generation of $e^{-\text{CB}}$ and $h^{+\text{VB}}$ when exposed to sunlight. The more the number of $e^{-\text{CB}}$ and $h^{+\text{VB}}$ the more will be the number of Cr(VI) ions reduced to Cr(III) ions, as a result % reduction increases with the increase in the particle concentration ([Figure 4\(c\)](#)). The opposite trend was observed for the M4 membrane for which the agglomeration of particles resulted in a decrease in the active surface area available for the photon to generate a greater number of $e^{-\text{CB}}$ and $h^{+\text{VB}}$. Thereby, a lesser number of Cr(VI) ions will be reduced to Cr(III) under otherwise identical conditions. Thus, membrane M3 with 0.2 wt% of TiO_2 loading was selected as the best membrane at which excellent results for flux, % rejection and % reduction were obtained. Hence this membrane will be used in further experiments.

Effect of particle size

Images in [Figure 5](#) depict the impact of particle size on the performance of nanocomposite membranes for particle loading of 2 wt% at pH 5, transmembrane pressure (ΔP) 300 kPa, and $[\text{Cr(VI)}]$ 20 ppm. A decline in flux from 285 to 265 $\text{L/m}^2\text{h}$

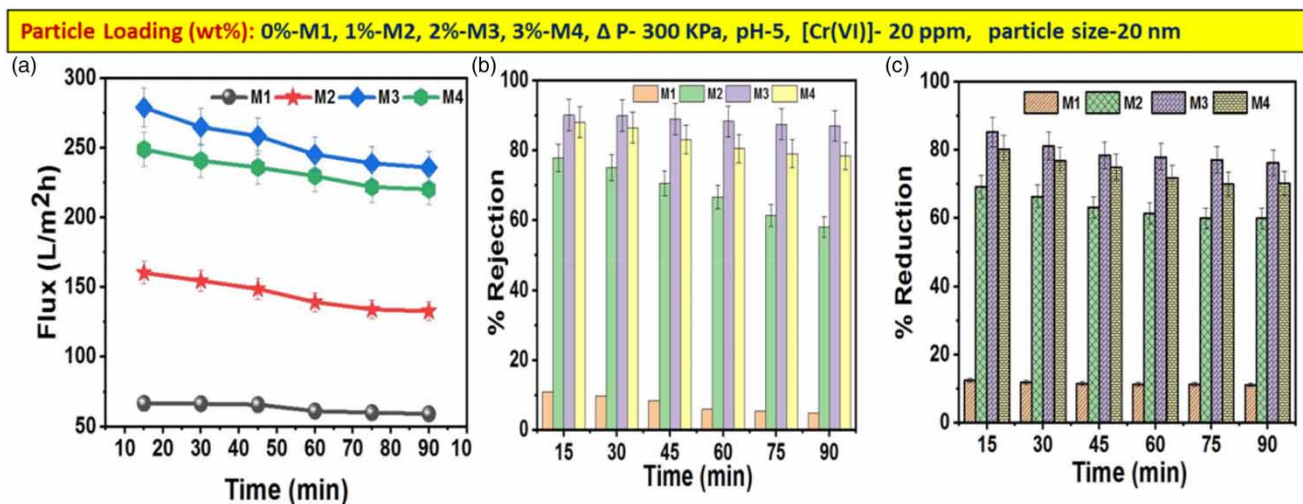


Figure 4 | Effect of NP loading. (a) Variation of flux, (b) % rejection, and (c) % reduction with time.

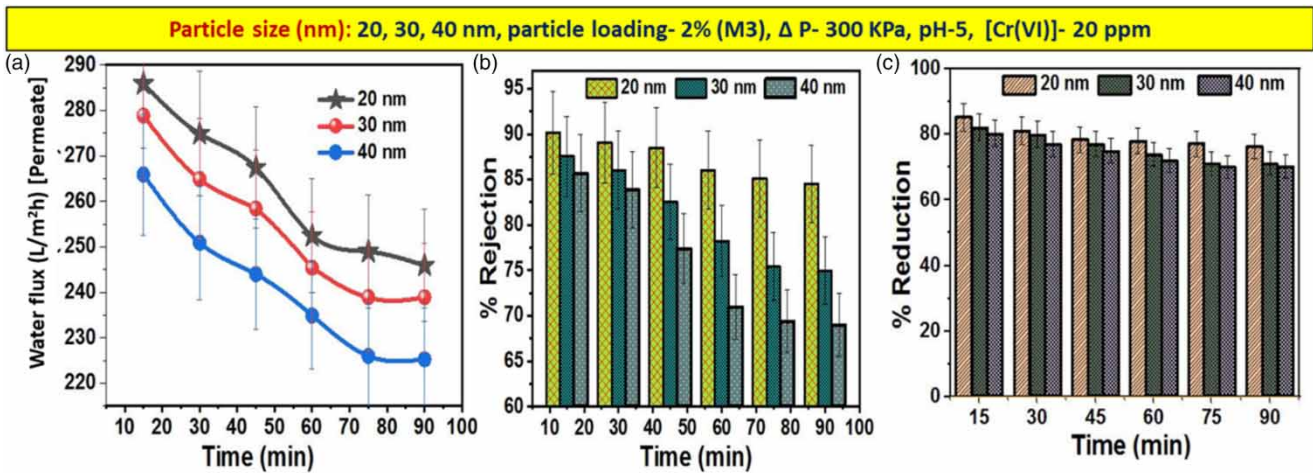


Figure 5 | Effect of particle size. (a) Variation of flux, (b) % rejection, and (c) % reduction with time.

approximately was observed as the particle size was increased from 20 to 40 nm, which was attributed to pore blockage of the membrane by the bigger size particles and also there will be a decrease in the number of pores per unit membrane area, due to which flux also decline. The Cr(VI) rejection was found to decrease with increase in particle size from 20 to 30 nm as shown in Figure 5(b), because the increased particle size will reduce the active surface area available for the ionic interaction to take place between the membrane and Cr ions at acidic pH. Similar results were also observed for % reduction (Figure 5(c)). The increased particle size reduces the active surface area available to generate large numbers of e^{-CB} and h^{+VB} to reduce Cr(VI) to Cr(III) form. Thus, it is seen that a large particle size is not preferable for good performance of the nanocomposite membrane. Thus, a particle loading of 2 wt%, and particle size 20 nm were selected as the best combination for excellent performance keeping all other parameters constant.

Effect of pH

Solution pH is a crucial parameter affecting the membrane performance in the rejection of Cr(VI) from the feed solution. Figure 6 depicts the variation in flux, % rejection and % reduction with respect to solution pH. The figure reveals the excellent performance at the acidic pH compared to basic pH. A change in the value of flux was observed from 100 to 280 L/m²h when the pH was changed from 9 to 3 (Figure 6(a)) attributed to the electrostatic interaction between chromium ions ($HCrO_4^-$) and

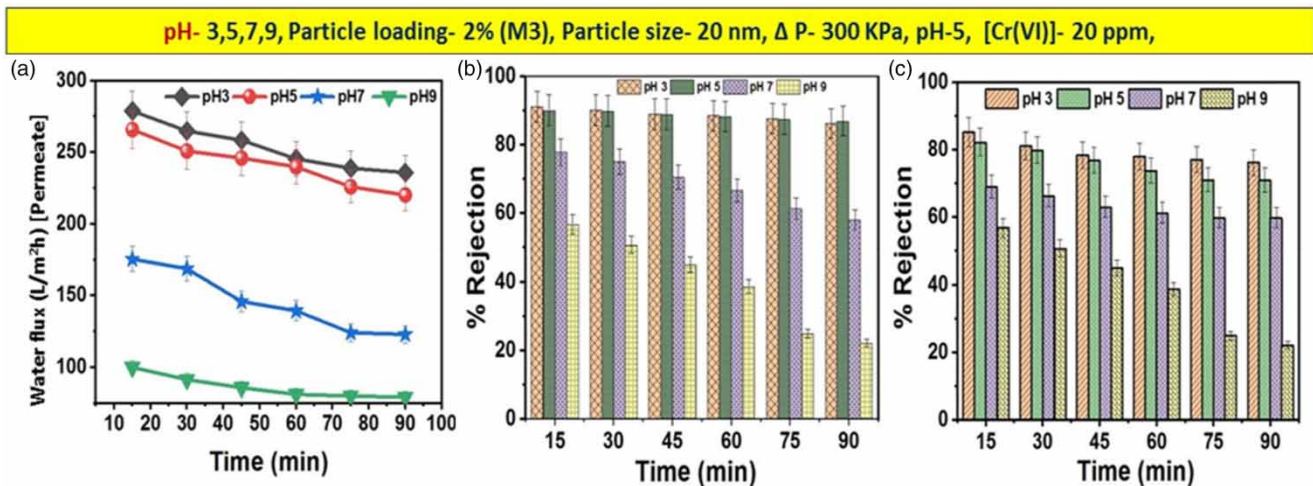


Figure 6 | Effect of pH. (a) Variation of flux, (b) % rejection, and (c) % reduction with time.

presence of TiO_2 as Ti-OH_2^+ in the polymer matrix, which will not allow Cr(VI) ions to become attached to Ti-OH_2^+ and will permit only water molecules to pass through it, hence there will be an increase in the water flux on the permeate side with decreasing pH. Furthermore, the values of water flux at pH 3 and 5 were nearly similar. Since the pH of chromium bearing wastewater from tanneries lies in the range pH 5–6, so pH 5 was selected as the best pH for achieving a high value of water flux on the permeate side under practical situations (Zhang *et al.* 2020). The presence of electrostatic forces between Cr ions ($\text{Cr}_2\text{O}_7^{2-}$, CrO_4^{2-} and HCrO_4^-) and Ti-OH_2^+ at acidic pH, produced a % rejection of Cr(VI) ions of >90% at pH 3 and 5, compared to 7 and 9 (Figure 6(b)). Under alkaline conditions, $\text{pH} > 7$, Cr(VI) exists as H_2CrO_4 therefore the interaction between the membrane and Cr ions in the feed solution is minimal, as a result the rejection is less (<60%) as observed at pH 9. Hence an acidic pH is preferred over basic pH for Cr(VI) ion removal from the feed solution. The same behaviour was observed for % reduction with time as shown in Figure 6(c) and favours acidic conditions for the photocatalytic reduction of Cr(VI) ion to Cr(III) ion. The study by Hudaya *et al.* (2013) explains that the reduction of Cr(VI) ion at low pH is thermodynamically favourable since the potential increases and is more positive than the conduction band of TiO_2 NPs.

Effect of Cr(VI) concentration

Chromium concentration in the feed solution is another important parameter affecting the membrane performance. Figure 7(a)–7(c) shows inverse relationship between flux, % rejection and % reduction with respect to concentration. The value of flux decreased from 280 to 170 $\text{L/m}^2\text{h}$ on increasing Cr(VI) concentration from 20 to 80 ppm (Figure 7(a)) because the increased concentration (at acidic pH, 2 wt % TiO_2 loading) results in excess Cr(VI) ions in the feed solution which will inhibit the passage of water molecules through the membrane and decrease the permeate side flux. Figure 7(b) shows that the %rejection decreased from 90 to 80% when the Cr(VI) concentration changed from 20 to 80 ppm because the membrane surface becomes saturated with Cr(VI) ions, which will affect the ionic interaction with the membrane due to the unavailability of Ti-OH_2^+ charge on the membrane. Also, the increased concentration will interfere with the light reaching the photocatalyst surface due to increased absorbance capacity at high concentrations thereby reducing the degree of reduction (Qamar *et al.* 2011), the same is observed in Figure 7(c).

Effect of transmembrane pressure

Transmembrane pressure is defined as the pressure gradient between permeate and feed sides. The more the gradient the more will be the solvent transfer, hence more will be the value of flux. Figure 8(a) shows the linear variation of flux with transmembrane pressure, which is expected. The increase in % rejection with increasing pressure is shown in Figure 8(b) and was attributed to the increase in convective transport of solvent (Riaz *et al.* (2016)). The other impact for better rejection at high pressure was due to the increase in permeate flux that may lead to the insignificant possibility of concentration polarization (Choudhury *et al.* 2018). Thus, at the loading of 2 wt%, particles of 20 nm size, at pH 5, and $[\text{Cr}]$ concentration of 20 ppm, 300 kPa was taken as the optimum pressure at which an excellent result would be obtained.

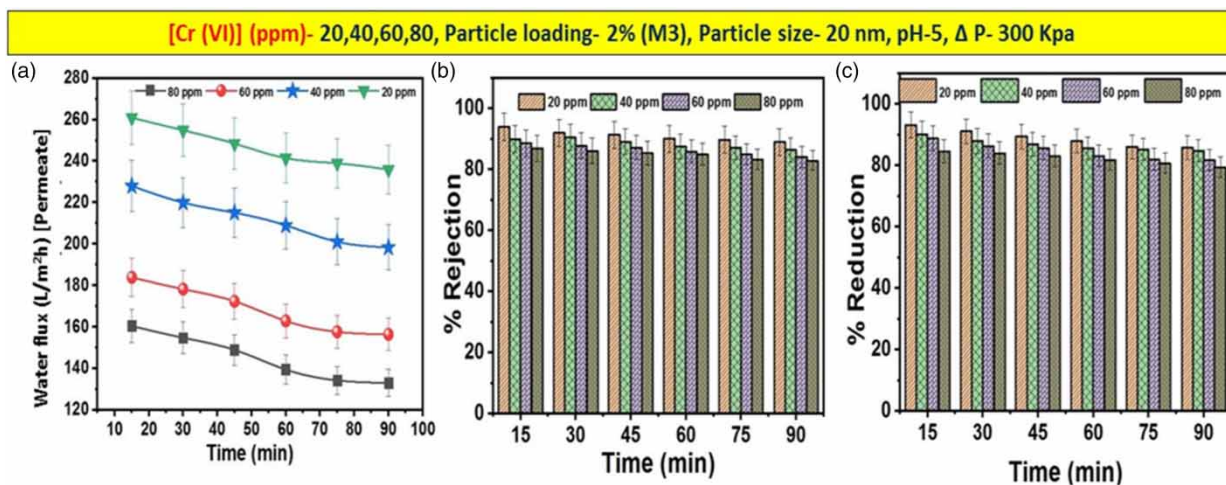


Figure 7 | Effect of $[\text{Cr(VI)}]$. (a) Variation of flux, (b) % rejection, and (c) % reduction with time.

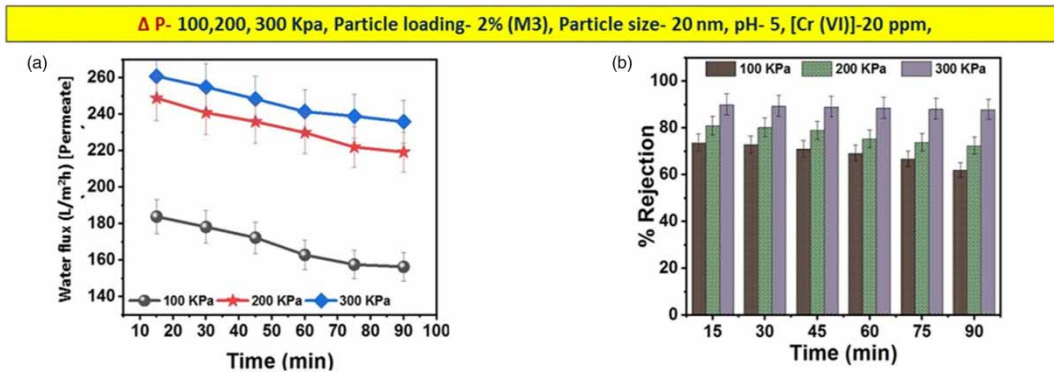


Figure 8 | Effect of transmembrane pressure. (a) Variation of flux, (b) % rejection with time.

RSM and ANOVA analysis

Data adequacy

The set of experiments was performed as suggested by RSM and the obtained data were analyzed using ANOVA. Figure 9(a) and 9(b) shows the response plots between actual versus predicted for % rejection and % reduction.

Here the experimentally determined values represent actual values, whereas the data obtained from the RSM model are referred to as predicted values. These plots determined the model adequacy and almost every point lies on the diagonal, which ensures the acceptability of the predicted values (Lu et al. 2009). The value of R² determines the model reliability. In this case, it was confirmed that experimental results fitted well with the predicted values because of the high value of R² and both responses followed the relation adjusted R² > Predicted R², i.e. for % rejection it is 0.9994 > 0.9980, and for % reduction, it corresponded to 0.9905 > 0.9617.

Effect of process variables on % rejection

RSM without any transformation suggested quadratic order for the regression analysis, and Equation (6) represents the RSM equation in terms of the actual factor including all the contributing factor of response

$$\begin{aligned} \% \text{ Rejection} = & 88.6458 + 39.226 * A + -0.919 * B + -1.551 * C + -0.3775 * AB + -1.7025 * AC \\ & + 0.155 * BC + -43.0945 * A^2 + -0.549545 * B^2 + -0.399545 * C^2 \end{aligned} \tag{8}$$

where A, B and C represent pH, particle loading and chromium concentration respectively.

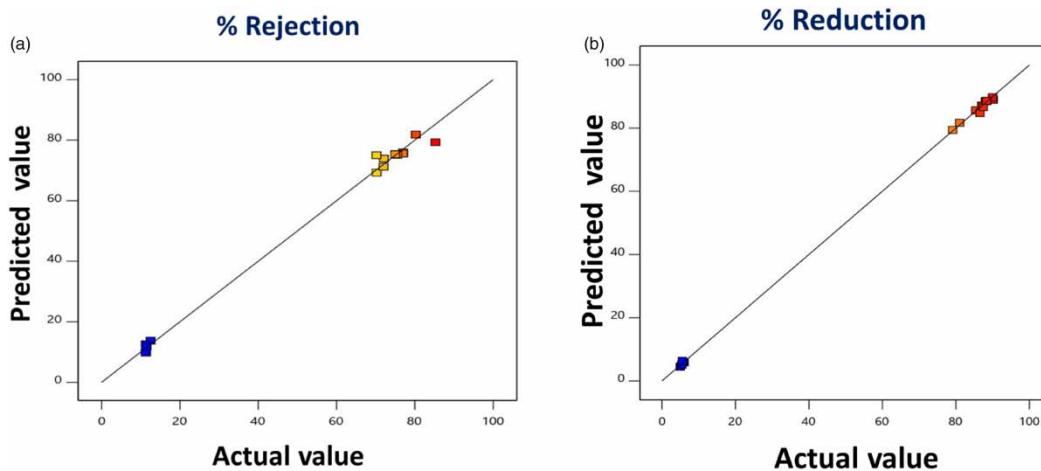


Figure 9 | Actual vs. predicted plot of the model: (a) % rejection (b) % reduction.

Model suitability and adequacy was determined using probability value (*p*-value) and Fisher’s statistical test (*F*-value) respectively. The model is statistically significant as *p*-value is less than 0.05 with a high *F*-value of 3,709.67 as mentioned in Table 2. At the same time in regression analysis, it is not mandatory to have all terms significant, even if *p*-values are less than 0.0500 it ensures that, as can be seen in Table 2, that linear terms namely, pH, particle loading, concentration, and quadratic term (particle loading)² are significant model terms.

The regression Equation (6) generates graphical response surfaces as shown by Figure 10. These plots explain the individual and combined effects of three independent variables on independent variables. The following conclusion be drawn from ANOVA analysis, i.e. pH parameter is a more significant followed by the concentration, and particle loading on % rejection of Cr(VI). A 3-D plot of response as a function of process variables is shown in Figure 10. Figure 10(a) and 10(b) shows a smaller value of % rejection at lower particle loading and the same trend was observed in the study carried out by Gasemloo *et al.* (2019) and Zhang *et al.* (2020) attributed to the lesser number of active sites available in the form of TiOH⁺ due to the low concentration and hence a lesser number of Cr(VI) ions will be rejected by the membrane. The opposite trend to that of particle loading was observed for responses on increasing the pH, as shown in Figure 10(b) and 10(c), which is due to the positive charge induced on the membrane surface in the presence of TiO₂ NPs and at low pH value in the presence of

Table 2 | ANOVA summary for % rejection from CCD model

Source	Sum of squares	df	Mean square	F-value	p-value	
Model	24,978.54	9	2,775.39	3,709.67	<0.0001	Significant
A	15,386.79	1	15,386.79	20,566.40	<0.0001	
B	8.45	1	8.45	11.29	0.0072	
C	24.06	1	24.06	32.15	0.0002	
AB	1.14	1	1.14	1.52	0.2453	
AC	23.19	1	23.19	30.99	0.0002	
BC	0.1922	1	0.1922	0.2569	0.6232	
A ²	5,107.13	1	5,107.13	6,826.33	<0.0001	
B ²	0.8305	1	0.8305	1.11	0.3169	
C ²	0.4390	1	0.4390	0.5868	0.4614	
Residual	7.48	10	0.7482			
Lack of fit	7.48	5	1.50			
Pure error	0.0000	5	0.0000			
Cor total	24,986.02	19				

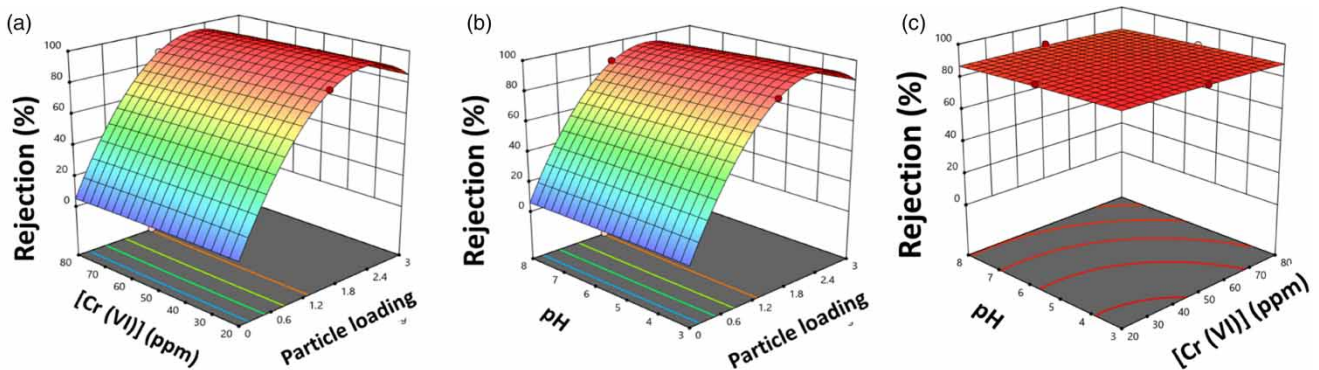


Figure 10 | 3D dimensional response surface of % rejection showing the effects of (a) particle loading and Cr(VI) concentration; (b) pH and particle loading; and (c) pH and Cr(VI) concentration.

Cr(VI) in anionic form (HCrO_4^-) at acidic pH that results in a strong electrostatic interaction, leading to increased Cr removal. A high Cr concentration is also not favourable to achieve high responses as can be seen in Figure 10(a) and 10(c) because, as already explained in Section 3.3.d, a high concentration generates an excess anionic charge on the membrane surface, thus creating a negative impact on the separation efficiency of membrane. These results concluded that all the three parameters, i.e. pH, particle loading, and Cr(VI) concentration, are important factors affecting the membrane performance.

Effects of process variables on % reduction

Equation (7) below represents the statistical equation for % reduction obtained using RSM:

$$\begin{aligned} \% \text{ Reduction} = & 75.3436 + 31.864 \times A + -2.137 \times B + -1.971 \times C + -0.49 \times AB + -1.695 \times AC \\ & + 0.31 \times BC + -31.6491 \times A^2 + 1.83591 \times B^2 + -2.14409 \times C^2 \end{aligned} \quad (9)$$

Similar to % rejection, here also ANOVA analysis ensured that the model was significant as the p -value is less than 0.0001 and the F -value is 220.43 (Table 3). Since the p -value is <0.05 for linear terms this implies a marked impact of these independent variables on the response.

The interaction between process and response variables is depicted by the 3-D plots as shown in Figure 11. The direct impact of particle loading photocatalytic reduction was observed and is shown in Figure 11(a) and 11(b). This means that particle loading plays a significant role because, as already stated, the increase in particle amount with respect to polymer weight there will result in a large number of electron and hole pair generations, which will accelerate the reduction of hexavalent chromium to the non-toxic form Cr(III). Figure 11(b) and 11(c) concludes that acidic pH is favourable for its excellent performance because variation in pH has a direct impact on the photoreduction process due to the presence of surface charge (Mohamed *et al.* 2016). Chromium concentration effect on % reduction is depicted in Figure 11(a) and 11(c) that shows that high concentrations will obstruct light reaching the photo-catalyst surface because of increased absorbance capacity, so the photoreduction efficiency decreases (Qamar *et al.* 2011). It can be thus concluded that pH, particle loading and concentration significantly affected both responses (% rejection and % reduction).

Optimization and validation of optimized results

The established quadratic equation was checked for optimization to determine the process variable values at optimum conditions to achieve maximization or minimization of the response output. In this case, the desired objective of the experimental design and optimization is keeping the two responses at 'maximum', whereas the desired goal is set as 'range'. The results of

Table 3 | ANOVA summary for % reduction

Source	Sum of squares	df	Mean square	F-value	p-value	
Model	15,346.40	9	1,705.16	220.43	<0.0001	Significant
A	10,153.14	1	10,153.14	1,312.54	<0.0001	
B	45.67	1	45.67	5.90	0.0355	
C	38.85	1	38.85	5.02	0.0489	
AB	1.92	1	1.92	0.2483	0.6290	
AC	22.98	1	22.98	2.97	0.1155	
BC	0.7688	1	0.7688	0.0994	0.7590	
A ²	2,754.58	1	2,754.58	356.10	<0.0001	
B ²	9.27	1	9.27	1.20	0.2993	
C ²	12.64	1	12.64	1.63	0.2300	
Residual	77.35	10	7.74			
Lack of fit	77.35	5	15.47			
Pure error	0.0000	5	0.0000			
Cor total	15,423.76	19				

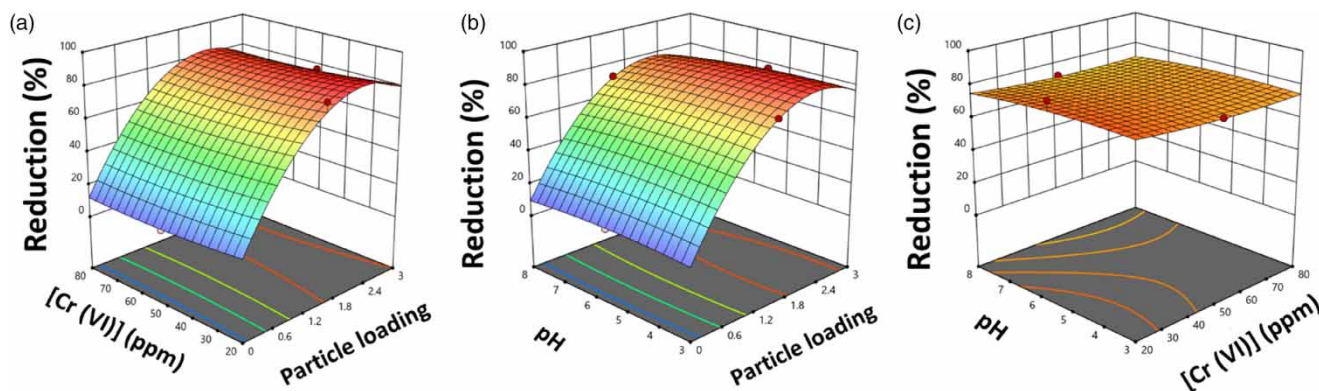


Figure 11 | 3D dimensional response surface and contour plots of % reduction showing the effect of (a) particle loading and Cr(VI) concentration, (b) pH and particle loading, and (c) pH and Cr(VI) concentration.

Table 4 | Predicted and experimental (actual) values at optimized conditions

	Loading (wt%)	[Cr(VI)] (ppm)	pH	Rejection (%)	Reduction (%)
Predicted	2.407	25.13	5.2	92.45	87.42
Observed	2.41	25	5.0	91.58	87.02

numerical optimization using the above model is tabulated in Table 4. To verify and validate the results an experiment was performed under the suggested optimum conditions. The results of the experiment conducted and RSM were consistent, hence this validates the findings with almost negligible percentage error obtained from the response surface optimization.

Reusability and stability

To investigate the reusability of the synthesized PVDF/TiO₂ membrane the experiment was run repeatedly five times, and the results are shown in Figure 12(a)–12(d) and Table 5. Data in Table 5 show elemental analysis of the membrane before and after the experiment. No drastic change in weight was observed for NPs in the composite membrane, which indicated particle stability in the polymer matrix. The results were further justified in Figure 12(a)–12(d) as no significant difference in the values of rejection and reduction were observed after five runs (Figure 12(a)) which confirms that the PVDF/TiO₂ membrane retains its reusable capacity. At the same time, there may be the possibility that particles may leach out in any of the runs if used continuously, so it becomes essential to ensure particle stability within the membrane. Determination of contact angle of the membrane is the simplest approach to indicate particle stability (Arif *et al.* 2019a). Figure 12(b) represents the contact angle values of the cleaned membrane after each run. Here also no differences in values were observed, which signified the excellent stability of the NPs within the host polymer.

Under acidic and neutral conditions, FTIR spectra for the composite membrane are shown in Figure 12(c). The figure concludes no existence/elimination of peaks in both environments. Peaks corresponding to wavenumber 1660 cm⁻¹ signified a hydroxyl group resulting from TiO₂ whereas 640 cm⁻¹ represents Ti-O-Ti bonds (Bhute *et al.* 2017). It can be concluded that the membrane retains its properties, as no morphological changes were observed in the acidic environment after application in the spectra. The morphological changes of composite film were further validated using the BET method.

The morphological changes before and after the application of composite film (first and last run) were analyzed using BET methodology as shown in Figure 12(d). The estimated BET surface area using the equation before and after membrane application was 383.5 and 366.7 m²/g, respectively. The obtained results further validated the recyclability of the synthesized PVDF/TiO₂ membrane since it retains its properties with minimum loss in the surface.

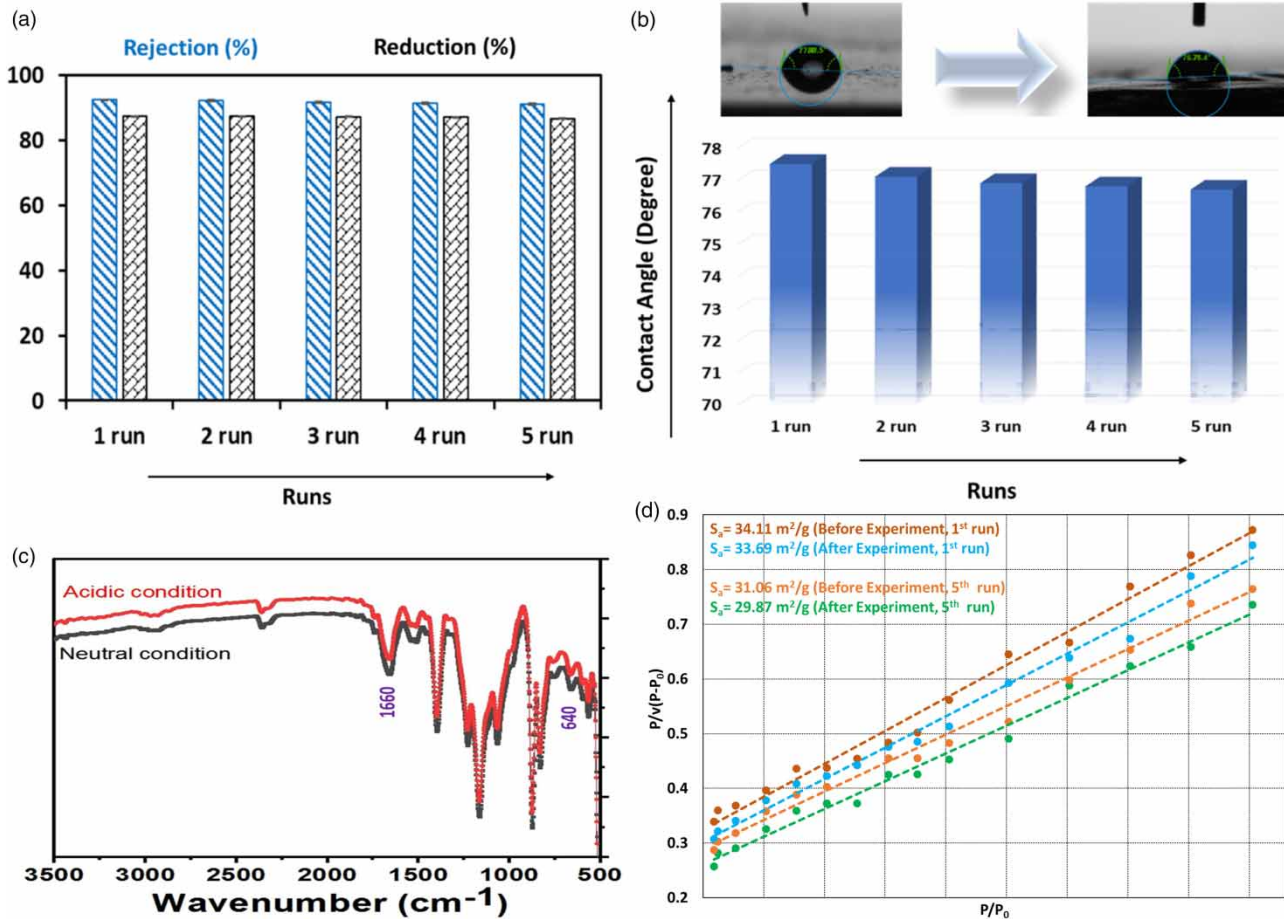


Figure 12 | Plots for (a) membrane reusability test; (b) contact angle value of the membrane after each run; (c) FTIR spectra for the membrane in the acidic and neutral conditions; and (d) BET plot of the pre- and post-applied membranes in the first and fifth runs.

Table 5 | Elemental analysis of composite membrane before and after experiment

	Before experiment (weight%)	After experiment (weight%)
C	42.68	42.71
F	56.07	55.9
Ti	1.25	1.19

CONCLUSION

The present investigation includes the use of a green approach, low cost PVDF/TiO₂ membrane for evaluating membrane performance in terms of % rejection and % reduction to eliminate toxic chromium (VI) metal from wastewater. The effects of parameters (pH, particle loading and size, metal concentration, transmembrane pressure) on the flux, rejection and reduction were studied to determine the suitable conditions for an excellent performance. A statistical tool, RSM was applied on a bi-functional ultra-filtration membrane to reduce the number of experiments to be conducted and to obtain optimal conditions and results which were validated by conducting the experiment under the given optimized conditions. Firstly, the experimental work suggested a 20 nm-sized particle with a loading of 2 wt% of TiO₂ in the polymer matrix at pH 5 and metal concentration of 20 ppm, the performance of membrane was excellent. Secondly, the response of interest was analyzed using RSM and the CCD models defining the reliability of the model since values of R² and R²_{adj} were greater than 0.95. Results obtained from CCD of RSM were predicted maximum theoretical values of 92.45% and 87.42% for Rejection and

reduction at optimum conditions and the nearly same values were obtained from the experiments. Thus, it can be concluded that a low cost bi-functional ultrafiltration membrane was developed successfully.

DATA AVAILABILITY STATEMENT

All relevant data are included in the paper or its Supplementary Information.

CONFLICT OF INTEREST

The authors declare there is no conflict.

REFERENCES

- Abba, M. U., Man, H. C., Azis, R. A. S., Isma Idris, A., Hazwan Hamzah, M., Yunos, K. F. & Katibi, K. K. 2021 Novel PVDF-PVP hollow fiber membrane augmented with TiO₂ nanoparticles: preparation, characterization and application for copper removal from leachate. *Nanomaterials* **11** (2), 399.
- Arif, Z., Sethy, N. K., Kumari, L., Mishra, P. K. & Verma, B. 2019a Antifouling behaviour of PVDF/TiO₂ composite membrane: a quantitative and qualitative assessment. *Iran. Polym. J.* **28**, 301–312.
- Arif, Z., Sethy, N. K., Kumari, L., Mishra, P. K. & Verma, B. 2019b Green synthesis of TiO₂ nanoparticles using *Cajanus cajan* extract and their use in controlling the fouling of ultrafiltration PVDF membranes. *Korean J. Chem. Eng.* **36** (7), 1148–1156.
- Arif, Z., Sethy, N. K., Mishra, P. K. & Verma, B. 2020a Green approach for the synthesis of ultrafiltration photocatalytic membrane for tannery wastewater: modeling and optimization. *Int. J. Environ. Sci. Technol.* **17**, 3397–3410.
- Arif, Z., Sethy, N. K., Mishra, P. K. & Verma, B. 2020b Development of eco-friendly, self-cleaning, antibacterial membrane for the elimination of chromium (VI) from tannery wastewater. *Int. J. Environ. Sci. Technol.* **17**, 4265–4280.
- Bhute, M., Mahant, Y. & Kondawar, S. 2017 Titanium dioxide/poly(vinylidene fluoride) hybrid polymer composite nanofibers as potential separator for lithium ion battery. *J. Mater. NanoSci.* **4**, 6–12.
- Burakov, A. E., Galunin, E. V., Burakova, I. V., Kucherova, A. E., Agarwal, S., Tkachev, A. G. & Gupta, V. K. 2018 Adsorption of heavy metals on conventional and nanostructured materials for wastewater treatment purposes: a review. *Ecotoxicol. Environ. Saf.* **148**, 702–712.
- Choudhury, P. R., Majumdar, S., Sahoo, G. C., Saha, S. & Mondal, P. 2018 High pressure ultrafiltration CuO/hydroxyethyl cellulose composite ceramic membrane for separation of Cr(VI) and Pb (II) from contaminated water. *Chem. Eng. J.* **336**, 570–578.
- Crini, G. & Lichtfouse, E. 2019 Advantages and disadvantages of techniques used for wastewater treatment. *Environ. Chem. Lett.* **17**, 145–155.
- Gasemloo, S., Khosravi, M., Sohrabi, M. R., Dastmalchi, S. & Gharbani, P. 2019 Response surface methodology (RSM) modeling to improve removal of Cr(VI) ions from tannery wastewater using sulfated carboxymethyl cellulose nanofilter. *J. Cleaner Prod.* **208**, 736–742.
- Hudaya, T., Marsha, A., Paramita, E., Shierin & Andean, D. 2013 Effect of pH and photocatalyst concentration on hexavalent chromium removal from electroplating waste water by UV/TiO₂ photocatalysis. *J. Appl. Sci.* **13** (4), 639–644.
- Jyothi, M. S., Vignesh, N., Mahesh, P., Balakrishna, R. G. & Soontarapa, K. 2017 Eco-friendly membrane process and product development for complete elimination of chromium toxicity in wastewater. *Hazard Mater.* **332**, 112–123.
- Lace, A., Ryan, D., Bowkett, M. & Cleary, J. 2019 Chromium monitoring in water by colorimetry using optimised 1,5-diphenylcarbazine method. *Int. J. Environ. Res. Public Health* **16**, 1803.
- Lu, S.-Y., Qian, J.-Q., Wu, Z.-G., Ye, W.-D., Wu, G.-F., Pan, Y.-B. & Zhang, K.-Y. 2009 Application of statistical method to evaluate immobilization variables of trypsin entrapped with sol-gel method. *J. Biochem. Technol.* **1** (3), 79–84.
- Mohamed, A., Osman, T. A., Toprak, M. S., Muhammed, M., Yilmaz, E. & Uheida, A. 2016 Visible light photocatalytic reduction of Cr(VI) by surface modified CNT/titanium dioxide composite nanofibre. *J. Mol. Catal A: Chem.* **424**, 45–53.
- Qamar, M., Gondal, M. A. & Yamani, Z. H. 2011 Synthesis of nanostructured NiO and its application in laser-induced photocatalytic reduction of Cr(VI) from water. *J. Mol. Catal A: Chem.* **341**, 83–88.
- Ramasundaram, S., Seid, M. G., Choe, J. W., Kim, E. J., Chung, Y. C., Cho, K., Lee, C. & Hong, S. W. 2016 Highly reusable TiO₂ nanoparticle photocatalyst by direct immobilization on steel mesh via PVDF coating, electrospraying, and thermal fixation. *Chem. Eng. J.* **306**, 344–351.
- Riaz, T., Ahmad, A., Saleemi, S., Adrees, M., Jamshed, F., Hai, A. M. & Jamil, T. 2016 Synthesis and characterization of polyurethane-cellulose acetate blend membrane for chromium (VI) removal. *Carbohydr. Polym.* **153**, 582–591.
- Sharma, G., Naushad, M., Muhtaseb, A., Kumar, A., Khan, R., Kalia, S., Bala, M. & Sharma, A. 2017 Fabrication and characterization of chitosan-crosslinked-poly (alginate acid) nanohydrogel for adsorptive removal of Cr(VI) metal ion from aqueous medium. *Int. J. Biol. Macromol.* **95**, 484–493.
- Zhang, S., Shi, Q., Korfiatis, G., Christodoulatos, C., Wang, H. & Meng, X. 2020 Chromate removal by electrospun PVA/PEI nanofibres: adsorption, reduction, and effects of co-existing ions. *Chem. Eng. J.* **387**, 124179–124188.